Bio-Sustainable Alternatives Synthesis of Nanoporous Activated Carbon @Al-MOF for the Adsorption of Hazardous Organic Dyes from Wastewater

H. M. Abd El Salam

Abstract The disposal of textile pollutants tainted by soluble organic dyes into the water without proper treatment may adversely impact the aquatic environment, humans, plants, and animals due to their toxic nature. As a result, the goal of this work is to look into the adsorptive removal of Eriochrome Black T (EBT) dye (as a model of soluble anionic organic dyes) from aqueous solution using a green synthesis nanoporous activated carbon @ Aluminum based metal–organic frameworks (AC@Al-MOFs) from a lemon peel waste as an inexpensive biosorbent. The physicochemical properties of Al-MOF and AC@Al-MOF composite were characterized by X-ray diffraction (XRD), Fourier transforms infrared spectroscopy (FTIR), Brunauer–Emmett–Teller (BET), scanning electron microscopy (SEM), and the impact of varied parameters on adsorption efficiency of Eriochrome Black T (EBT) including pH, dye concentrations, contact time and adsorbent dose, was examined. The experimental isotherms data were analyzed using Langmuir and Freundlich isotherm equations. The best fit was obtained by the Langmuir model with high correlation coefficients ($R^2 = 0.9976$) with a maximum monolayer adsorption capacity of 303.0 mg/g. The results suggest that AC@Al-MOF composite is a potential choice for removing EBT dye molecules from aqueous media.

1 Introduction

Environmental contamination is one of the biggest issues facing current life. During various stages of the dyeing and finishing processes, which make up a considerable portion of textile manufacturing, dyes pollute a lot of water. Pharmaceuticals, plastics, papers, printing, food, and leather industries are some of the additional industries that use dyes in diverse processes (Monvisade & Siriphannon, 2009; Ayub et al., 2018; Crini, 2006; Mittal et al., 2007; Chen et al., 2010). Major dyes made from azo, thioquinone, and xanthan have been deemed the most significant industrial organic pollutants because they are non-biodegradable, extremely toxic, and carcinogenic. Examples of these dyes include methylene blue,

Highlights
- Green activated carbon/Aluminum- based metal organic framework composite was synthesized in water.
- AC@Al-MOF was used for the adsorption of EBT dye as an adsorbent from aqueous media.
- Physicochemical mechanisms influenced the adsorption process.
- Adsorption mechanisms for EBT on AC@Al-MOF were suggested as potential mechanisms.

H. M. Abd El Salam (✉)
Analysis and Evaluation Division, Egyptian Petroleum Research Institute, Nasr City, PO Box 11727, Cairo, Egypt
e-mail: Howaida.abdelsalam@gmail.com

methyl orange, rhodamine B, crystal violet, and congo red (Tahir et al., 2020; Shindhal et al., 2021; Dassanayake et al., 2021). A serious risk to both the aquatic ecosystem and human health exists when azo dye-containing wastewater is improperly or ineffectively treated because azo dyes have one or more azo (-N=N-) groups within their structure, which significantly contributes to their toxicity, carcinogenicity, and genotoxicity to living organisms (Xiaoming et al., 2014; Monvisade & Siriphannon, 2009; Barka et al., 2011; Mohammadi et al., 2011; Lin et al., 2004; Ejhieh & Khorsandi, 2010; Ahmed & Hameed, 2010). Some azo dyes have the potential to cause cancer without cleaving into aromatic amines. However, many azo dyes' carcinogenicity is caused by their cleavage products, such as benzidine. Various cancer in both people and animals have been caused by benzidine. Benzidine is known as a carcinogen for the human urinary bladder (Armina et al., 2019). There are a number of strategies available for the removal of dyes, such as membrane separation, coagulation, ozonation, electrochemical coagulation, and adsorption, which have been developed to successfully and efficiently capture azo dyes from wastewater before they reach the environment (Arshadi et al., 2014; Joanna et al., 2014). Adsorption processes are still to be the most attractive techniques, due to their simplicity, low or no formation of secondary contaminants, ease of operation, great cost-effectiveness, and high selectivity (Hu et al., 2016; Ran et al., 2016; Zhang et al., 2013). Recently, metal–organic frameworks (MOFs) are considered the pioneer compounds in material and scientific applications due to their unique properties, such as high porosity, surface area, an abundance of active sites at the metal nodes, and flexibility in framework (Meipeng et al., 2015; Abd El Salam & Zaki, 2018; Asmaa et al., 2020; Abd El Salam et al., 2017). Despite advancements, MOFs were unsuitable for environmental remediation since they were not as stable in moist conditions. As a result, the modification of MOF materials has become an issue of concern in order to overcome these drawbacks. For instance, by doping additional functionalized materials (such as graphene, magnetic microspheres, and metal ions) into the MOF for creating a unique hybrid material (Huang et al., 2018). Activated carbon is a porous material that contains 85 to 95% carbon. Natural materials available may be used in the activated carbon adsorption technique as inexpensive

adsorbents. In several operations, activated carbon generated from rice husks, lemon peels, orange peels, banana peels, and other organic materials have been used successfully (Juhaina et al., 2016). Activated carbon (AC) has great potential for the preparation of composites because of its unique laminar structure and surface characteristics. In addition, it may be easily dispersed in water or other polar solvents because of its good hydrophilic characteristics (Shaobin et al., 2011). It was well-accepted that AC/MOF composites would enhance the dispersion force and generate new void spaces (Jabbari et al., 2016). Although numerous efforts have been made the removal of different aquatic contaminants, a few reports have been published on the disposal of anionic azo dyes from the aquatic environment (Fangna et al., 2017; Kyung et al., 2018a, b). The synthesis of new adsorbents that can be synthesized in a more "green" solution to minimize the negative impacts and create platforms for the cost-effective synthesis of the adsorbent for dye removal. In this paper, Al-MOF and biomass AC@Al-MOF composite were synthesized and characterized, and its removal of Eriochrome Black T (EBT) from wastewater was also been investigated. The physicochemical experiments, mechanisms, and regeneration have also been studied.

2 Materials and Methods

2.1 Materials

Aluminum nitrate nonahydrate (Al $(NO_3)_3 \cdot 9H_2O$) was purchased from Merck and succinic acid ($C_4H_6O_4$) was purchased from Sigma-Aldrich Korea. The Lemon Peels were collected from a waste obtained after complete lemon juice extraction, Eriochrome Black T (EBT ($C_{20}H_{12}N_3NaO_7S$) and potassium hydroxide (KOH) from Merck. All the chemicals were used without further treatment.

2.2 Synthesis of Lemon Peel Activated Carbon

The Lemon Peels were collected from a waste obtained after complete lemon juice extraction and these were washed with water to eliminate dust and impurities. Dried in the oven at 105 °C overnight to remove extra water content and grinded into fine powder. Lemon peels were soaked in KOH solution

with an impregnation ratio (Lemon Peels: KOH) of 1:1 and kept at room temperature for 24 h to ensure the penetration of the KOH to the Lemon Peel. Filter the solution and dried at 500 °C for 2 h. Thus, activated carbon is produced.

2.3 Synthesis of Nanoporous AC@Al-MOF Composite

In this study, AC@Al-MOF was synthesized in situ by the synthesis of Al-MOF in the presence of AC according to the following procedure. $Al(NO_3)_3.9H_2O$ (5.2 mmol) was dissolved in 100 mL of deionized water and (25 mg) of activated carbon was added then, the solution was stirred at 60 °C for 1 h. (5.3 mmol) of succinic acid and (8.5 mmol) of NaOH were added to 100 mL of deionized water. The solution containing succinic acid was slowly poured into the first solution containing aluminum precursor and activated carbon. The mixture was stirred at 60 °C for 3 h, followed by separation using centrifugation. The obtained solid was washed thoroughly using deionized water to remove any residual impurities. Finally, the final product was dried at 100 °C overnight.

2.4 Characterization of the Synthesized Nanoporous AC@Al-MOF Composite

Powder X-ray diffraction (XRD) examination was performed with a PAN analytical X'PERT, PRO employing CuKα X-ray radiation (λ = 1.540) to examine the surface crystallinity. Quanta-chrome Nova 3200 S automated gas sorption device was used to calculate textural properties of the adsorbent (the specific surface area) using N_2 adsorption–desorption isotherms at liquid nitrogen temperature (-196 °C). The sample was perfectly degassed at 120 °C for an overnight period prior to measurements, with a vacuum pressure of 1.3×10^{-3} Pa. Fourier transform infrared (FT-IR) spectroscopy from Perkin Elmer was used to identify and determined the functional groups and chemical moieties of the adsorbent in the range 4000–400 cm^{-1} (model spectrum one FT-IR spectrometer, USA). The standard KBr pellets were used to prepare the samples. To evaluate the surface morphology of AC@Al-MOF, scanning electron microscopy (SEM) was done on a Quanta 250 field emission gun (FEG) attached to an EDS unit at a 30 kV accelerating voltage.

2.5 Adsorption Experimental Methods

The experimental EBT dye concentrations were obtained by dilution of a prepared stock solution (1000 mg/L). The influence of solution pH on the adsorption of EBT was appreciated through the pH of the stock solutions of EBT was adjusted within the range of 3.0 to 10.0 using a pH meter with (0.1 M of HCl and NaOH). 0.01 g of Al-MOF and AC/Al-MOF were immersed into 20 ml of solutions containing 50 mg/L of EBT. The solutions were put in Erlenmeyer flasks at 200 rpm and 25 °C for 180 min. The remaining concentrations of the dyes in the supernatant solutions were estimated by UV–Vis spectroscopy using at 530 nm. The removal efficiency (R %) and amount of adsorbed EBT dye (q_e, mg/g) were calculated according to the following equations:

$$R\% = \left(\frac{Co - Ce}{Co} \right) \times 100 \tag{1}$$

$$qe = \frac{V(Co - Ce)}{M} \tag{2}$$

where C_o and C_e are the initial and equilibrium EBT concentrations (ppm), V is the volume of solution (L), and m is the adsorbent mass (gm).

The studied initial concentration of EBT was achieved in the range of 50 to 200 mg/L at pH 4 for 0.01 gm of adsorbent material was placed into 20 mL of EBT solution at 25 °C for 180 min. 0.01 gm of synthesized samples (Al-MOF and AC@Al-MOF) and 20 ml of 50 mg/L EBT were used to evaluate the influence of contact time at pH 4. Finally, the solution was collected and the corresponding amount of EBT adsorbed was calculated using Eq. (2). To evaluate the role of the adsorbent dose, the amounts of Al-MOF and AC@Al-MOF from 0.01 to 0.1g were added to 20 ml 50 mg/L dye solution at equilibrium duration of 180 min.

3 Results and Discussion

3.1 Characterization of Al-MOF and AC@Al-MOF Composite

The crystal structure and lattice parameters of Al-MOF, AC, and AC@Al-MOF were determined by XRD analysis and the XRD spectrum is presented in Fig. 1. According to Fig. 1b, an amorphous structure was obtained due to the activated carbon phase

(AC) from bio-waste of lemon peel and determined the characteristic phase belongs to activated carbon at $2\theta = 26°$ and $42°$ are attributed to (002) and (100) planes (Zehra et al., 2019).

As shown in Fig. 1a indicating that Al-MOF distinguishes two sharp peaks located at $2\theta = 11.5°$ and $22.7°$ correspond to 011 and 022 reflections with their corresponding d-spacing values being 7.3 Å and 3.1 Å, which has good crystallinity and a good agreement with previously reported literature (Kyung et al., 2018a, b). Al-MOF and AC@Al-MOF diffraction patterns were almost identical, indicating that the
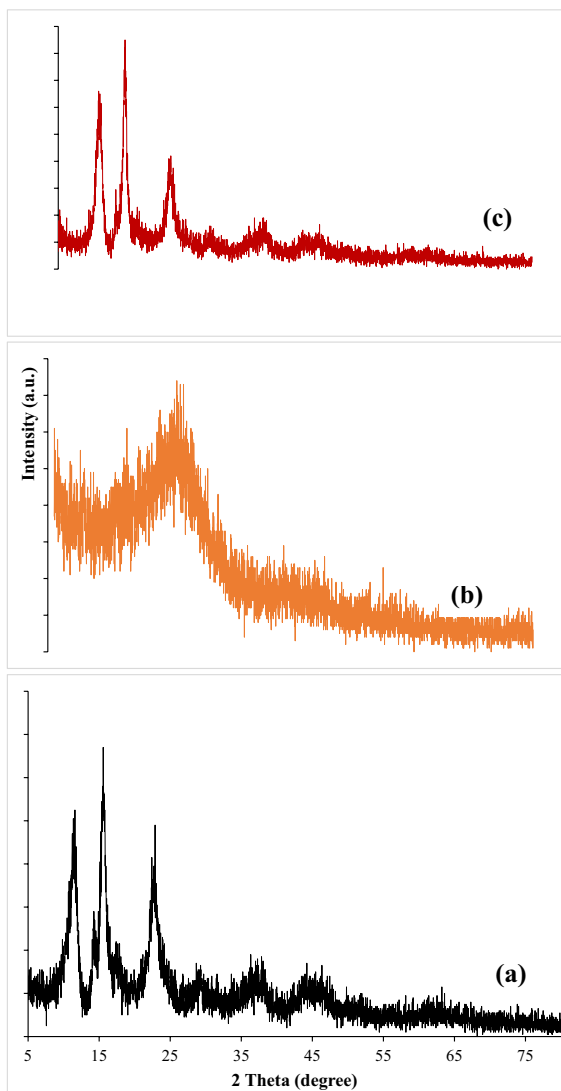
Al-MOF crystal structure is not harmed by the addition of AC, due to the in situ growth and associated incorporation of the Al-MOF with the AC surface. In addition, the diffraction peak intensity of AC@Al-MOF was slightly weaker than that of the parent material Al-MOF, demonstrating that the addition of AC slightly impacted the crystallization of Al-MOF, resulting in small significant deformation of the structure. The nitrogen adsorption–desorption isotherms for Al-MOF and AC@Al-MOF composite are illustrated in Fig. 2. Both samples' isotherms exhibit common type IV isotherms with an H3-typical hysteresis loop that corresponds to mesoporous materials. The evaluated BET surface area of Al-MOF and AC@Al-MOF composite was found to be 146.73 and 105.43 m^2/g, respectively. The difference in the total pore volume of Al-MOF and AC@Al-MOF from 0.231 to 0.276 cm^3g^{-1}. This might be a result of the creation of a new channel between AC and Al-MOF (Kyung et al., 2018a, b; Rowe & Kraft, 2009).

Figure 3a, c shows the FTIR spectra of Al-MOF and AC@Al-MOF. A sharp peak around 3700 cm^{-1} represents $AlO_4(OH)_2$ octahedral nodes (Mani et al., 2015). The band at 3500 cm^{-1} corresponds to water molecules present within the prepared Al-MOF sphere. Carboxylate group (COO^- asymmetric and symmetric) stretching vibrations are represented by the bands at 1600 and 1500 cm^{-1} (Hueeein et al., 2016). Bands between 450 and 1150 cm^{-1} are featured characteristics of Al-O vibrations in octahedral geometry (Kyung et al., 2018a, b). Figure 3b shows the FTIR spectra of the activated carbon synthesized from bio-waste lemon peel. Sharp peaks at 3400 cm^{-1} (–OH stretch), 2800 cm^{-1} (C–H stretch), 1700 cm^{-1} (C=O stretch), 1200 cm^{-1} (C-O stretch), 1300 cm^{-1} and 1400 cm^{-1} (C–H bend) clarify the presence of alkanes; 1100 cm^{-1} (C-H bend) and 1600 cm^{-1} (C=C stretch) suggests the presence of alkenes (Brij et al., 2021).

Figure 3c illustrates that AC@Al-MOF nanocomposite's drop in band intensity at 1615 cm^{-1} (carboxylic acid C-O group) and the appearance of a new absorption band at 1710 cm^{-1} (ester carbonyl group) confirm the possibility that succinic acid, acting as a ligand, may react with activated carbon. The hydroxyl stretching vibration of AC and the carbonyl group of succinic acid, respectively, are represented by the peaks at 3410 cm^{-1} and 1680 cm^{-1}, respectively. It was predicted that the reaction between AC

Fig. 1 XRD patterns of the synthesized Al-MOF (**a**), AC (**b**), and AC@Al-MOF composite (**c**)

Fig. 2 Nitrogen adsorption isotherms for Al-MOF and AC@Al-MOF composite
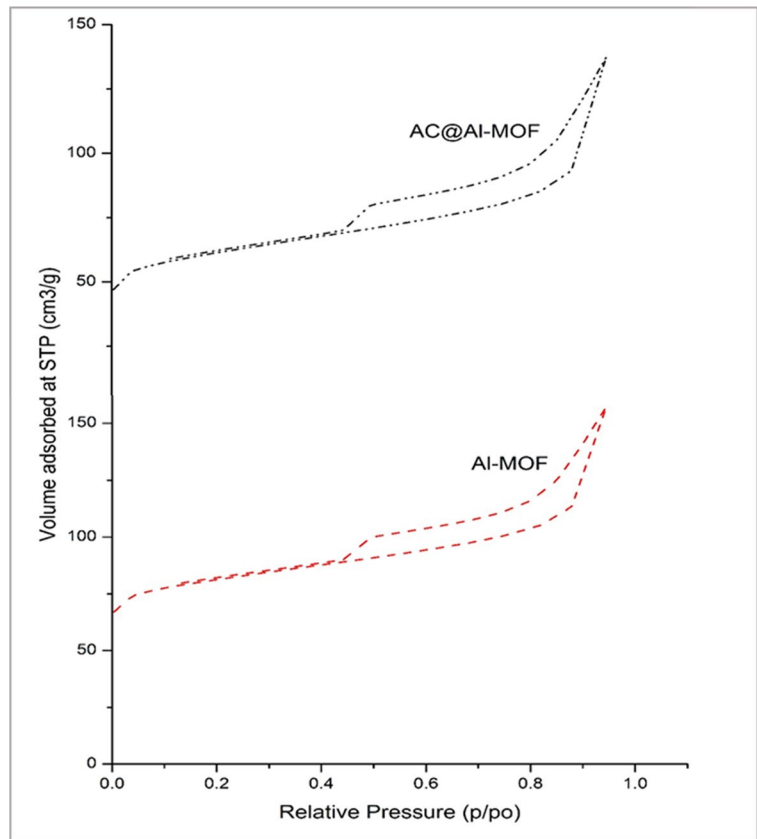
and succinic acid would result in the formation of an ester carbonyl group at 1710 cm^{-1}.

Figures 4a, b displays the surface morphology (SEM) of Al-MOF and AC@Al-MOF. The SEM image for Al-MOF showed a smooth surface, whereas AC@Al-MOF displayed a porous structure like a sponge. The porosity of the AC@Al-MOF composite is fruitful for fast ion diffusion (Li et al., 2015; Surya & Michael, 2021). The results of the SEM study of AC@Al-MOF are in approval with that of adsorption isotherm studies.

3.2 Adsorption Activity of EBT Using Al-MOF and AC/Al-MOF
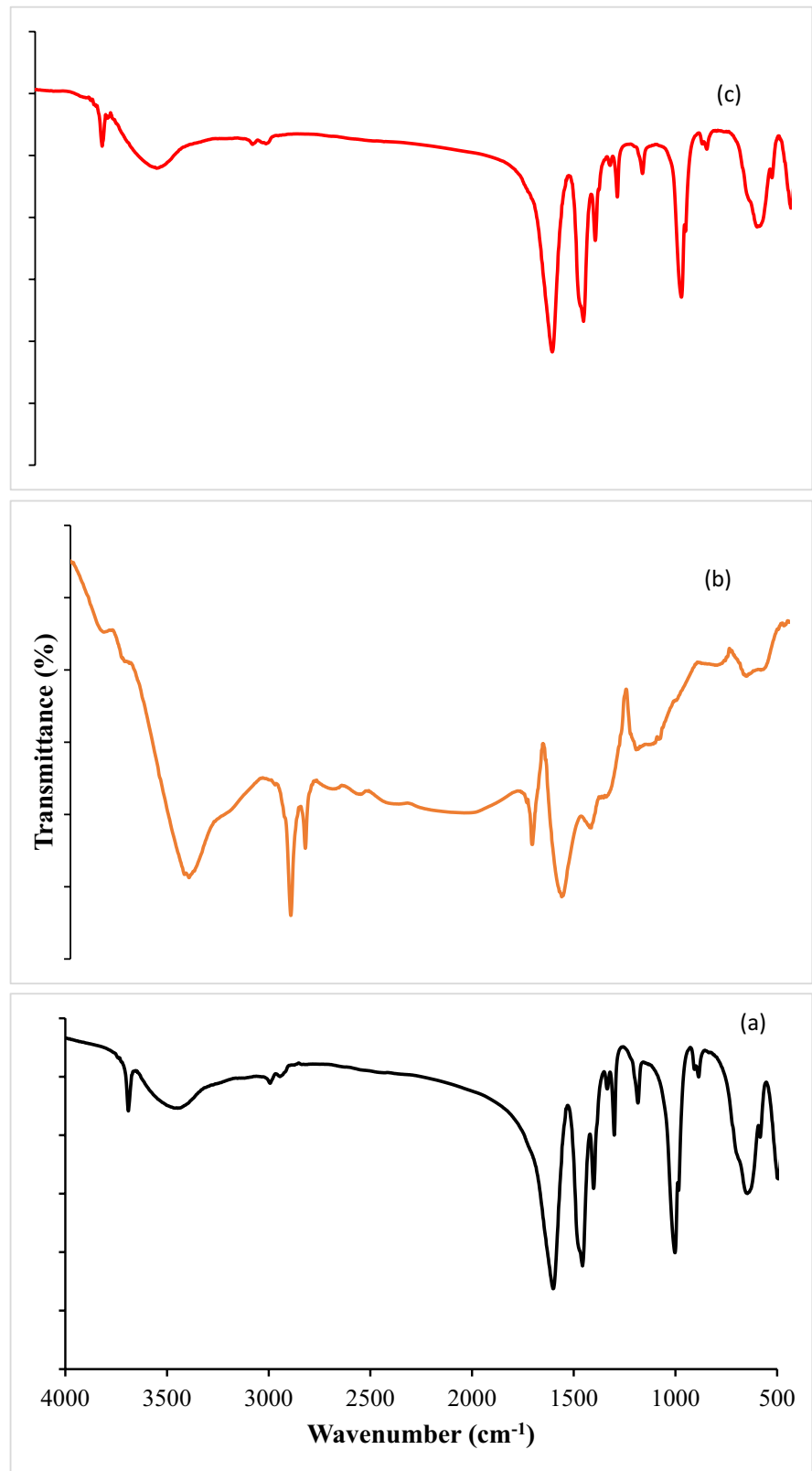
3.2.1 Effect of pH

The pH has a significant impact on the removal of textile dyes by changes in differential charges on both the adsorbate surface and the adsorbent. The synthesized AC-based Al-MOF composite has a positively charged surface, which generates electrostatic adsorption between the adsorbent and adsorbate. As indicated in Fig. 5, AC@Al-MOF demonstrates a remarkable affinity for EBT elimination with adsorption capacities exceeding 276 mg/g (>95% removal rate). Although there is a significant decrease as the media's pH increase as a result of the deprotonation of hydroxyl groups at the metal nodes. The adsorption of EBT on AC@Al-MOF showed comparable results as well microwave-assisted spent black tea leaves (MASTL) (Ayub et al., 2018).

3.2.2 Effect of Initial EBT Concentration and Adsorption Isotherm

To evaluate the adsorption strength of synthesis Al-MOF and AC@Al-MOF towards the adsorption of EBT dye from aqueous solutions at different concentrations (50, 100, 150, 200 ppm). The removal percentage of EBT decreased from 96 to 44% and 83 to 31% for AC@Al-MOF and Al-MOF, respectively, with an increase in concentration from 50 to 200 ppm attributed to insufficiency of active sites to accept more EBT dye available in the solution. The

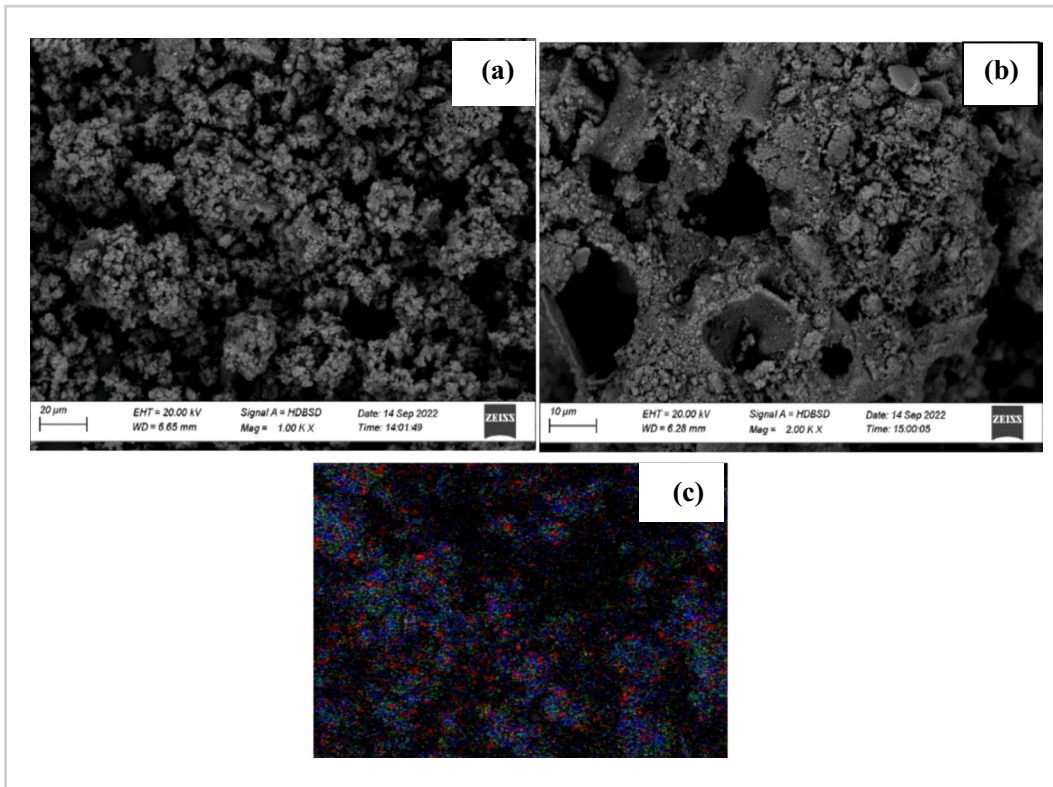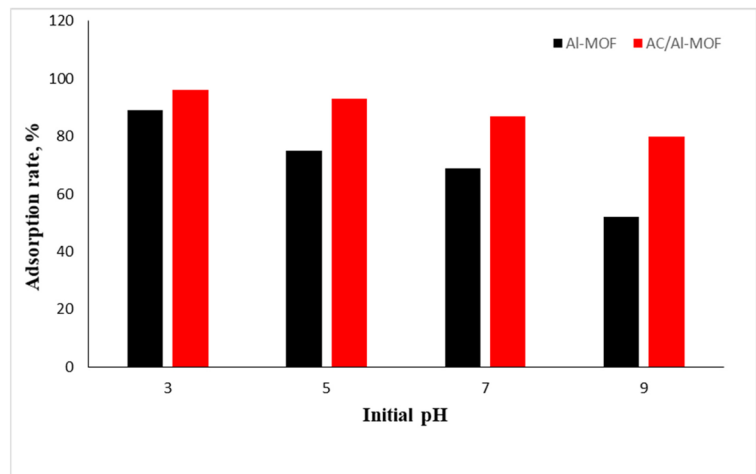**Fig. 3** FTIR spectra of Al-MOF (**a**), AC (**b**), and AC@Al-MOF composite (**c**)

Fig. 4 SEM images of Al-MOF (**a**), AC@Al-MOF (**b**), and elemental mapping AC@Al-MOF (**c**)

Fig. 5 Effect of pH on the decolonization of EBT over Al-MOF and AC@Al-MOF composite, dye concentrations (50 mg L.$^{-1}$); temperature (25 °C); Al-MOF &AC@Al-MOF dosage, (0.01 g); volume (20 mL); contact time (3 h)

adsorption isotherms can be determined by applying the Langmuir (3) and Freundlich (4) equations in a linear form.

$$\frac{1}{q_e} = \frac{1}{C_e q_m k_L} + \frac{1}{q_m} \tag{3}$$

$$\ln(q_e)\ln(k_F) + \frac{1}{n}\ln(C_e) \tag{4}$$

where C_e (ppm) represents the solute equilibrium concentration, q_e (mg g^{-1}) represents the amount of solution adsorbed per unit mass of the adsorbent, q_m
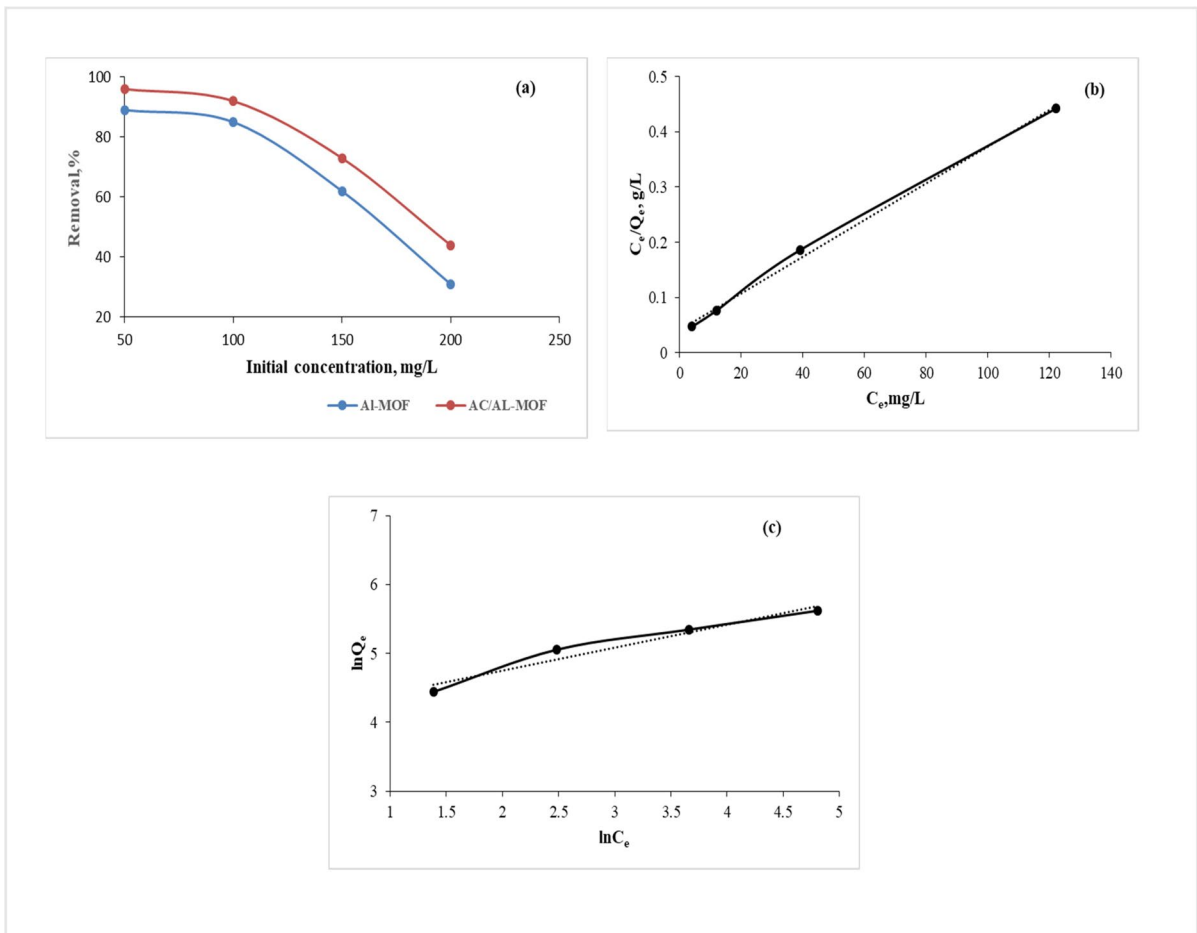
Fig. 6 Adsorption removal % of Al-MOF and AC@Al-MOF composite for different concentrations of EBT (**a**), Langmuir isotherms (**b**), and Freundlich isotherms (**c**)

Table 1 Adsorption isotherm parameters

Adsorbents	$Q_{m,\text{exp}}$ (mg/g)	Adsorption isotherms					
		Langmuir equation			Freundlich equation		
		q_m (mg/g)	k_L (L.mg^{-1})	R^2	K_F (mg.g^{-1})	n	R^2
AC@Al-MOF	276	303	0.351	0.9976	82	2.53	0.9403

(mg g^{-1}) represents the maximum adsorption capacity, and k_L (L mg^{-1}) represents the Langmuir constant. The Freundlich constants for adsorption capacity and intensity, respectively, are k_F (mg$^{-1/n}$ L$^{-1/n}$ g^{-1}) and n, respectively.

Figure 6b, c illustrates that the Langmuir isotherm model has a higher linear fit than the Freundlich isotherm model which can be applied for homogenous surfaces and mono-layer adsorption.

Table 1 shows values of q_m and R_L calculated from the slope and the intercept. In this research, the Langmuir isotherm model's R^2 value was approximately 1. Accordingly, it has been demonstrated that AC/Al-MOF is an appropriate adsorbent for the removal of EBT from aqueous solutions and the adsorption of EBT has been successfully explained through the Langmuir isotherm (Vesna et al., 2014).
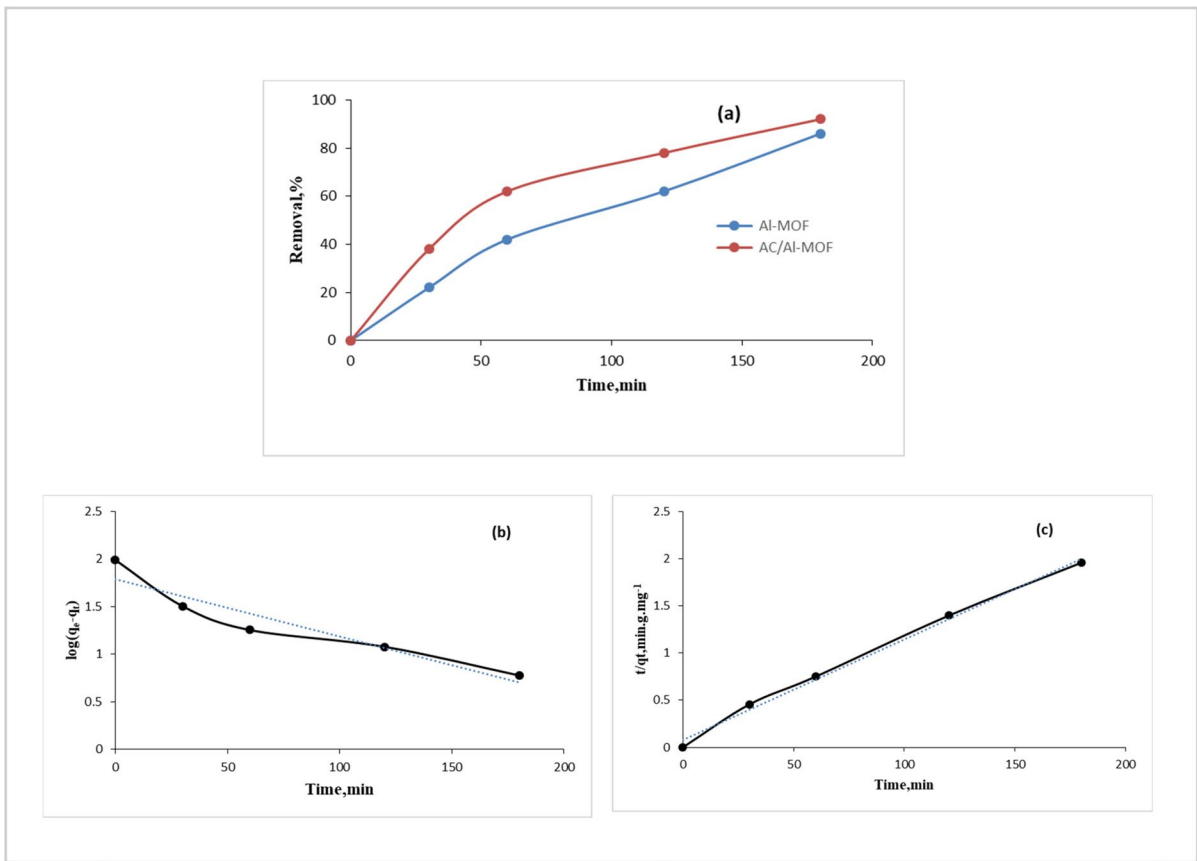
Fig. 7 Effect of contact time on the adsorption % of EBT on Al-MOF and AC@Al-MOF composites (**a**); pseudo-first order (**b**), and pseudo-second order (**c**) on AC@Al-MOF(pH 4.0; temperature 25 °C; Al-MOF &AC@Al-MOF dosage 0.01 g; volume 20 ml)

Table 2 Kinetic parameters for EBT adsorption

| Adsorbents	$q_{e,\exp}$ (mg/g)	Pseudo-first-order kinetics model			Pseudo-second-order kinetics model		
		q_e (mg/g)	k_1 (min^{-1})	R^2	q_e (mg/g)	k_2 (mg/(g min))	R^2
AC@Al-MOF	260.06	249.81	0.0352	0.8968	255.41	0.0015	0.9944

3.2.3 Effect of Contact Time and Adsorption Kinetics

The effect of contact time was examined to explain the adsorption equilibrium state for maximum uptake and to demonstrate the kinetics of adsorption process. The adsorption experiments on Al-MOF and AC@Al-MOF were tested as a function of contact times ranging from 0 to 180 min. The results are shown in Fig. 7. The results show that the adsorption rate of EBT increased sharply after the first 30 min to reach 22% for Al-MOF and 38% for AC@Al-MOF. The highest activity of the adsorption EBT was achieved after 2 h to reach 92% for AC@Al-MOF sample and then it reaches to the equilibrium after 180 min (Mahdi et al., 2020). To understand the adsorption kinetics of AC@Al-MOF, mainly two kinetic models, pseudo-first order and pseudo-second order models, were used for the experimental data.

$$\text{Pseudo} - \text{first} - \text{order } \log(q_e - q_t) = \log(q_e) - k_1 t \tag{5}$$

Fig. 8 Absorption spectra of EBT solution at different time on AC@Al-MOF
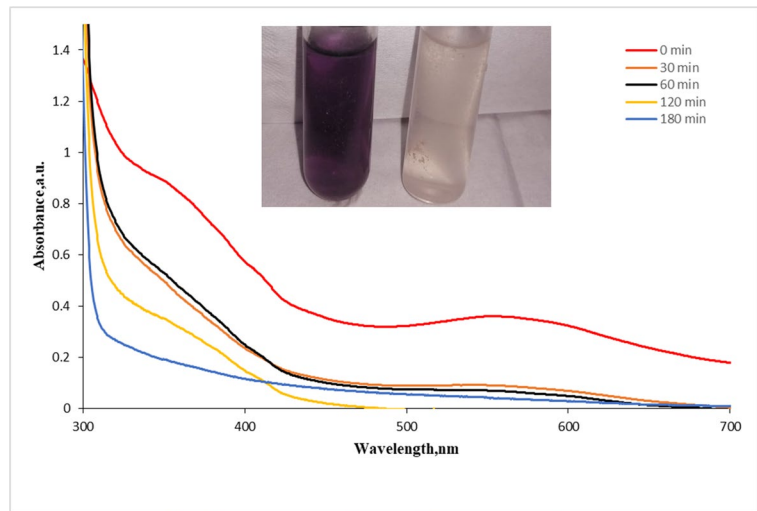
Pseudo − second − order $\frac{t}{q_t} = \frac{1}{k_2 q_e^2} + \frac{t}{q_e}$ (6)

where q_e (mg g^{-1}) is the quantity of EBT adsorbed at equilibrium and q_t (mg g^{-1}) is the amount of EBT adsorbed at the time (t). The pseudo-first-order and pseudo-second-order rate constants for the adsorption mechanism are k_1 and k_2, respectively. The values of q_e and k_1 are calculated from the intercepts and slopes of the plot Fig. 7b corresponding to Eq. (5), which are given in Table 2. The low-related coefficient ($R^2 = 0.8968$) and the large difference between the calculated values of adsorption capacity and the experimental values indicate that the sorption mechanism of EBT on the AC@Al-MOF sample does not fit a

pseudo-first-order kinetic model well. Figure 7c shows straight lines of the pseudo-second-order model with correlation coefficients ($R^2 = 0.9944$) for the AC@Al-MOF sample. Therefore, the adsorption kinetic fits the pseudo-second-order model, this could be due to dye species easily diffusing through the porous nature of the MOF and the adsorption kinetics of AC@Al-MOF conforms to the pseudo-second-order model (Huang et al., 2019) (Fig. 8).

3.2.4 Effect of Adsorbent Amount

EBT dye uptake capacity increased rapidly with the increasing amount of adsorbent from 0.01 to

Fig. 9 Effect of adsorbent amount on the adsorption % of EBT on Al-MOF and AC@Al-MOF (pH 4.0; temperature 25 °C; contact time 3 h; volume 20 mL)
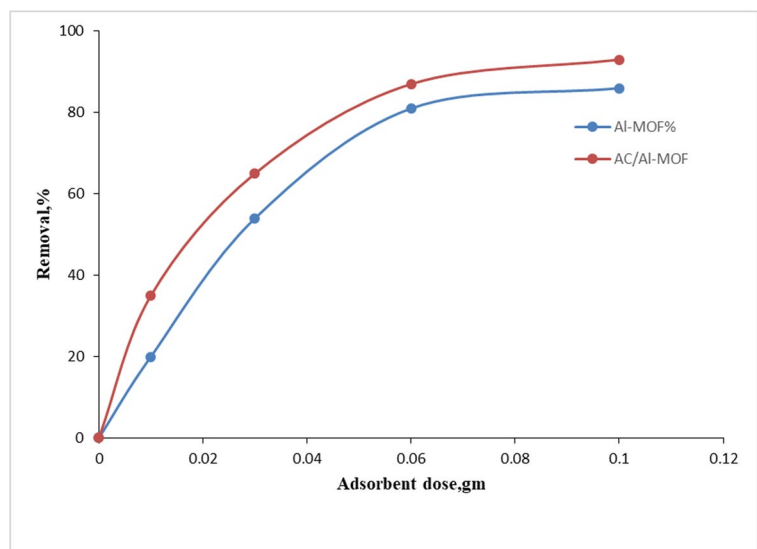
0.1 g/L, EBT concentration of 50 mg/l, and a constant agitation speed (200 rpm). At this time, as the amount of adsorbent increased, more surface area and active sites became available for adsorption, allowing more EBT dye to be removed. This could be because the adsorption sites remain unsaturated during the adsorption reaction but finally become saturated as the adsorbent concentration rises. On the other hand, the uptake of the EBT dye was found to be 25% Al-MOF and 38% AC@Al-MOF at catalyst amount 0.01 g L^{-1} and increased to 86% and 94% at 0.05 g for Al-MOF and AC@Al-MOF, respectively (Fig. 9).
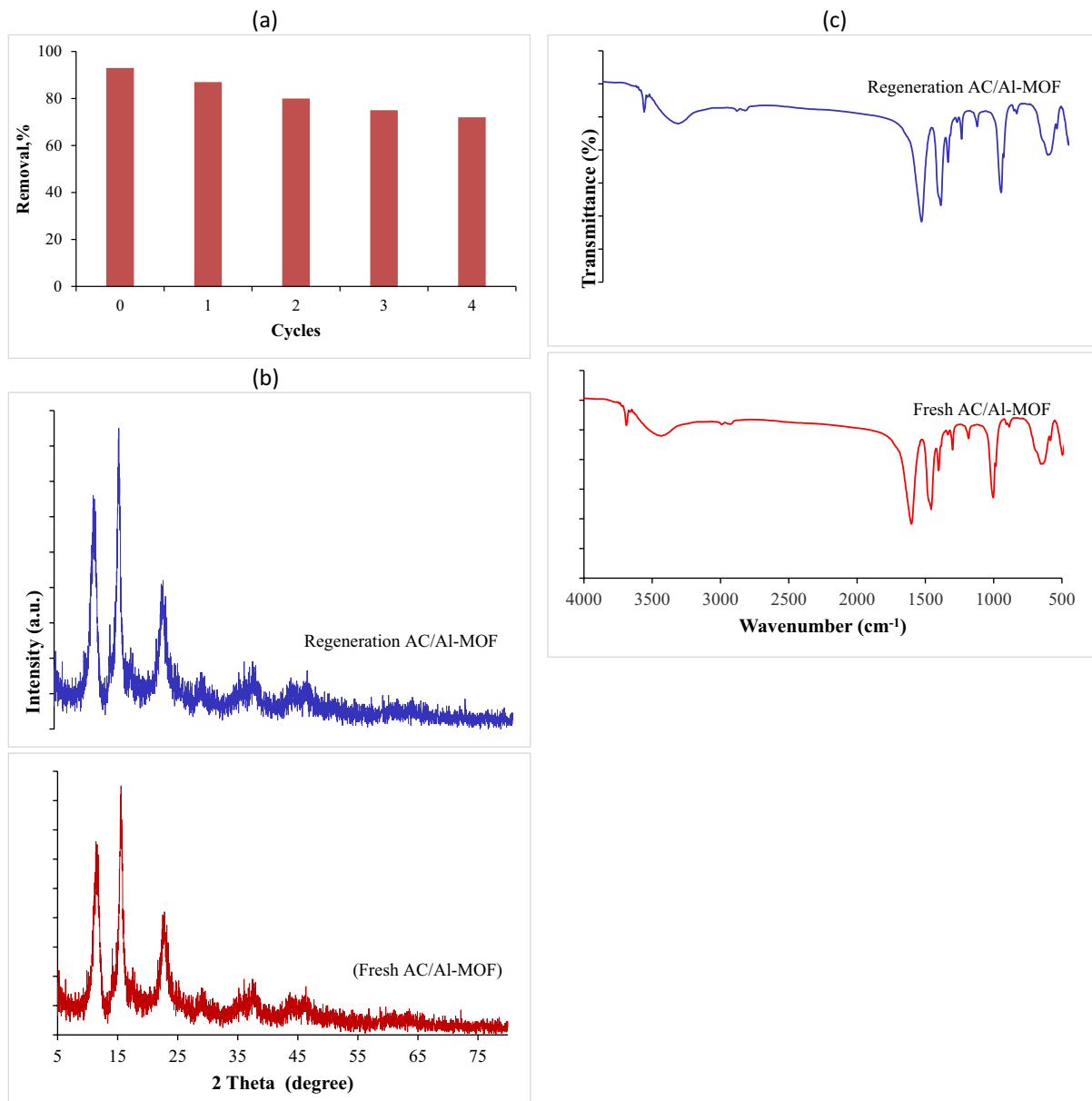

Fig. 10 Regeneration of AC@Al-MOF for EBT removal (**a**), XRD patterns (**b**), and the FTIR (**c**) of regenerated AC@Al-MOF (contact time = 180 min, dye concentrations = 50 mg L.$^{-1}$, dose = 0.01g/L, temperature = 25 °C, pH = 4)

Table 3 Comparison of maximum removal adsorption effects through different adsorbents

Adsorbents	Removal, %	References
UiO-66 and UiO-66 modulated with acetic acid	98.06	(Pambudi et al., 2021)
Waste activated sludge	97.08	(Mohamed et al., 2018)
Nanoporous activated carbon @Al-MOF	96	**Present study**
Activated carbon prepared from waste rice hulls	95.91	(Mark et al., 2013)
Tea waste	95	(Megha et al., 2020)
Zeolitic imidazolate frameworks (ZIFs)	92.5	(Gholam et al., 2020)
NiFe2O4 magnetic nanoparticles	91	(Moeinpour et al., 2014)
Acid-modified graphene	80	(Arsalan, et al., 2018)

There are references for each specified the significance of bold entries

3.2.5 AC@Al-MOF Regeneration

Regeneration is one of the benefits of adsorption processes for satisfying both economic and environmental. In this study, to evaluate the reusability of AC@Al-MOF, ethanol was employed to desorb EBT from the sample. The adsorption reaction over the prepared AC/Al-MOF was carried out for four cycles at the same reaction condition; at 25 °C for 3 h in the presence of AC@Al-MOF dosage 0.01 g; volume 20 mL and pH 4.0. As illustrated in Fig. 10a, the adsorption capacity of the adsorbent was reduced to reach 78% after the four cycles, which confirmed that AC@Al-MOF can easily separate, and has great stability and durability. AC@Al-MOF did not significantly lose its efficiency and selectivity after the four cycles during the adsorption EBT reaction (Fig. 10b, c), demonstrating that AC@Al-MOF is an effective adsorbent with potential for azo dye adsorption and can be used again.

3.2.6 Adsorption Mechanism

Due to the existence of various functional groups in EBT, including amino, sulfonate, and nitro groups, the adsorption behavior of Al-MOF and AC@Al-MOF composite on EBT involved electrostatic interaction, π-π stacking, and hydrogen bonding interaction. Under acidic conditions, Al-MOF and AC@Al-MOF were positively charged, and EBT was negatively so, electrostatic attractions can be generated among the functional groups and electron cloud at the metal node. Additionally, succinate linkers can increase the van der Waals interaction between the aromatic rings of EBT and the linker's hydrocarbon chains, which improves the adsorbate-adsorbent interaction (Kyung et al., 2018a, b) (Table 3).

4 Conclusion

In the present work, Al-MOF and AC@Al-MOF, have been synthesized and employed for removing the azo dye EBT. The experimental data demonstrated that the adsorption efficiency of AC@Al-MOF was significantly higher than that of the parent Al-MOF. Therefore, the addition of AC managed to improve the EBT adsorption performance. Adsorption isotherms have revealed that both chemical and physical adsorption occurred.

Declarations

Conflict of Interest The author declares no competing interests.

References

Abd El Salam, H. M., & Zaki, T. (2018). Removal of hazardous cationic organic dyes from water using nickel-based metal-organic framework. *Inorganica Chimica Acta, 471*, 203–210.

Abd El Salam, H. M., Younis, S. A., Ali, H. R., & Zaki, T. (2017). Statistical modeling and optimization of phenol adsorption from water by modified $Cu_3(BTC)_2$: Kinetic, isotherm, and thermodynamic analysis. *Microporous and Mesoporous Materials, 241*, 210–217.

Ahmad, A., & Hameed, B. (2010). Fixed-bed adsorption of reactive azo dye onto granular activated carbon prepared from waste. *Journal Hazardous Materials, 175*, 298–303.

Armina, G., Lamija, H. & Alma, K. (2019). Toxicity of azo dyes in pharmaceutical industry. *International Conference on Medical and Biological Engineering*, 581–587, https://doi.org/10.1007/978-3-030-17971-7_88

Arsalan, Kh., Mukarram, Z., & Ihsanullah. (2018). A comparative study on the adsorption of Eriochrome Black T dye from aqueous solution on graphene and acid-modified graphene. *Arabian Journal for Science and Engineering, 43*, 2167–2179.

Arshadi, M., SalimiVahid, F., Salvacion, J. W. L., & Soleymanzadeh, M. (2014). Adsorption studies of methyl orange on an immobilized Mn-nanoparticle: Kinetic and thermodynamic. *Royal Society of Chemsitry Advances, 4*, 16005–16017.

Asmaa, S. M., El S Howaida, A., El N Ahmed, M. A., & Tamer, Z. (2020). Hydrogen production and in-situ storage through process of water splitting using mono/ binary metal organic framework (MOF) structures as new chief photocatalysts. *Energy Fuels, 34*, 11660–11669.

Ayub, K., Xiangke, W., Kashif, G., Fazli, K., Zaynab, A., & Elseman, A. M. (2018). Microwave-assisted spent black tea leaves as cost-effective and powerful green adsorbent for the efficient removal of Eriochrome black T from aqueous solutions. *Egyptian Journal of Basic and Applied Sciences, 5*, 171–182.

Barka, N., Abdennouri, M., & Makhfouk, M. E. L. (2011). Removal of Methylene Blue and Eriochrome Black T from aqueous solutions by biosorption on Scolymus hispanicus L.: Kinetics, equilibrium and thermodynamics. *Journal Taiwan Institute Chemical Engineers, 42*, 320–326.

Brij, B., Arunima, N., & Shreya, K. (2021). Green synthesis of highly porous activated carbon from jackfruit peel: Effect of operating factors on its physico-chemical characteristics. *Materials Today: Proceedings, 44*, 187–191.

Chen, S., Zhang, J., Zhang, C., Yue, Q., Li, Y., & Li, C. (2010). Equilibrium and kinetic studies of methyl orange and methyl violet adsorption on activated carbon derived from Phragmites australis. *Desalination, 252*, 149–156.

Crini, G. (2006). Non-conventional low-cost adsorbents for dye removal: A review. *Bioresource Technology, 97*, 1061–1085.

Dassanayake, R. S., Acharya, S., & Abidi, N. (2021). Recent advances in biopolymer-based dye removal technologies. *Molecules, 26*(15), 4697–4716.

Ejhieh, A. N., & Khorsandi, M. (2010). Photodecolorization of Eriochrome Black T using NiS– P zeolite as a heterogeneous catalyst. *Journal Hazardous Materials, 176*, 629–637.

Fangna, D., Weidong, F., Xue, Y., Zhaodi, H., Yutong, W., Xuelian, X., Huan, L., Liangliang, Z., Rongming, W., & Daofeng, S. (2017). A non-interpenetrating lead-organic framework with large channels based on 1D tube-shaped SBUs. *Chemical Communications, 53*, 5694–5697.

Gholam, A. H., Shahram, S., Mohammad, H. S., Seid, K. G., Ioannis, A., Dimitrios, A. G., Juan, C. C., & Mahmoud, S. (2020). Zeolitic imidazolate frameworks (ZIFs) of various morphologies against eriochrome black-T (EBT): Optimizing the key physicochemical features by process modeling. *Colloids and Surfaces A, 606*, 125391.

Hu, M. L., Hashemi, L., & Morsali, A. (2016). Pore size and interactions effect on removal of dyes with two lead (II) metal-organic frameworks. *Materials Letters, 175*, 1–4.

Huang, L., He, M., Chen, B., & Hu, B. (2018). Magnetic Zr-MOFs nanocomposites for rapid removal of heavy metal ions and dyes from water. *Chemosphere, 199*, 435–444.

Huang, T. T., Yan, M., He, K., Huang, Z. Z., Zeng, G. M., Chen, A., Peng, M., Li, H., & Chen, G. Q. (2019). Efficient removal of methylene blue from aqueous solutions using magnetic graphene oxide modified zeolite. *Journal Colloid Interface Science, 543*, 43–51.

Hussein, R. A., Zana, H. R., Jin, Sh., & Shaobin, W. (2016). Synthesis, characterization, and CO_2 adsorption of three metal-organic frameworks (MOFs): MIL-53, MIL-96, and amino-MIL-53. *Polyhedron, 120*, 103–111.

Jabbari, V., Veleta, J. M., Zarei-Chaleshtori, M., Gardea-Torresdey, J., & Villagrán, D. (2016). Green synthesis of magnetic MOF@GO and MOF@CNT hybrid nanocomposites with high adsorption capacity towards organic pollutants. *Chemical Engineering Journal, 304*, 774–783.

Joanna, G., Michał, M., & Robert, P. (2014). Mesoporous carbons modified with lanthanum(III) chloride for methyl orange adsorption. *Chemical Engineering Journal, 247*, 258–264.

Juhaina, J.MAl.-F., Dinesh, K., & Elansezhian, R. (2016). Synthesis of activated carbon using orange and lemon peel for wastewater treatment application. *International Journal of Modern Science and Technology, 1*, 178–182.

Kyung, W. J., Brian, HCh., Chau, M. D., Young, J. L., Jae, WCh., Kyu, H. A., & Sang, H. L. (2018a). Aluminum carboxylate-based metal organic frameworks for effective adsorption of anionic azo dyes from aqueous media. *Journal of Industrial and Engineering Chemistry, 59*, 149–159.

Kyung, W. J., Brian, HCh., Seon, Y. L., Kyu, H. A., & Young, J. L. (2018b). Green synthesis of aluminum-based metal organic framework for the removal of azo dye Acid Black 1 from aqueous media. *Journal of Industrial and Engineering Chemistry, 67*, 316–325.

Li, Z., Lv, W., Zhang, C., Li, B., Kang, F., & Yang, Q. H. (2015). A sheet-like porous carbon for high-rate supercapacitors produced by the carbonization of an eggplant. *Carbon, 92*, 11–14.

Lin, S. H., Juang, R. S., & Wang, Y. H. (2004). Adsorption of acid dye from water onto pristine and acid-activated clays in fixed beds. *Journal Hazardous Materials, 113*, 195–200.

Mahdi, H., Abdolreza, S., & Hossein, S. F. (2020). Nanoporous composites of activated carbon-metal organic frameworks for organic dye adsorption: Synthesis, adsorption mechanism and kinetics studies. *Journal of Industrial and Engineering Chemistry, 81*, 405–414.

Mani, M. R., Chellaswamy, R., Marathe, Y. N., & Pillai, V. K. (2015). Role of the molecular structure of carboxylate-alumoxanes on the enhanced nucleation of polypropylene. *Chemical Communications, 51*, 10026–10029.

Mark, D. G. D. L., Edgar, D. F., Divine, A. D. G., Cybelle, M. F., & Meng-Wei, W. (2013). Adsorption of Eriochrome Black T (EBT) dye using activated carbon prepared from waste rice hulls—Optimization, isotherm and kinetic studies. *Journal of the Taiwan Institute of Chemical Engineers, 44*, 646–653.

Megha, B., Prem, K. P., & Tom, D. (2020). Adsorption of Eriochrome Black-T(EBT) using tea waste as a low cost adsorbent by batch studies: A green approach for dye effluent treatments. *Current Research in Green and Sustainable Chemistry, 3*, 100036.

Meipeng, J., Bao, L., Gaosheng, Z., Ruiping, L., & Xiwang, Z. (2015). Adsorptive removal of arsenic from aqueous solution by zeolitic imidazolate framework-8 (ZIF-8) nanoparticles. *Colloids and Surfaces A: Physicochemical and Engineering Aspects, 465*, 67–76.

Mittal, A., Malviya, A., Kaur, D., Mittal, J., & Kurup, L. (2007). Studies on the adsorption kinetics and isotherms for the removal and recovery of Methyl Orange from wastewaters using waste materials. *Journal of Hazardous Materials, 148*, 229–240.

Moeinpour, F., Alimoradi, A., & Kazemi, M. (2014). Efficient removal of Eriochrome black-T from aqueous solution using NiFe2O4 magnetic nanoparticles. *Journal of Environmental Health Science and Engineering, 12*, 112–118.

Mohamed, A.A.-E., Abeer, A.M.E.-S., Dalia, M. S. A. S., & Gehan, M. E. Z. (2018). The uptake of Eriochrome Black T dye from aqueous solutions utilizing waste activated sludge: Adsorption process optimization using factorial design. *Egyptian Journal of Aquatic Research, 44*, 179–186.

Mohammadi, N., Khani, H., Gupta, V. K., Amereh, E., & Agarwal, S. (2011). Adsorption process of methyl orange dye onto mesoporous carbon material-kinetic and thermodynamic studies. *Journal Colloid and Interface Science, 362*, 457–462.

Monvisade, P., & Siriphannon, P. (2009). Chitosan intercalated montmorillonite: Preparation, characterization and cationic dye adsorption. *Applied Clay Science, 42*, 427–431.

Pambudi, M. A. R., Prayogo, N. P., Ediati, R., Zulfa, L. L., & Nadjib, M. (2021). Study of UiO-66 and UiO-66modulatedwith acetic acid as the adsorbent for Eriochrome Black T Dye. *Indonesian Journal of Chemical Research, 8*(3), 186–193.

Ran, B., Feifei, Ch., Jie, L., Wei, L., & Feng, Y. (2016). Adsorption capability for anionic dyes on 2-hydroxyethyl-ammonium acetate-intercalated layered double hydroxide. *Colloids and Surfaces A: Physicochemical and Engineering Aspects, 511*, 312–319.

Rowe, M. D., & Kraft, T. S. L. (2009). Polymer-modified gadolinium metal-organic framework nanoparticles used as multifunctional nanomedicines for the targeted imaging and treatment of cancer. *Biomacromolecules, 10*, 983–993.

Shaobin, L., Tingying, H. Z., Mario, H., Ehdi, B., Jun, W., Rongrong, J., Jing, K., & Yuan, C. (2011). Antibacterial activity of graphite, graphite oxide, graphene oxide, and reduced graphene oxide: Membrane and oxidative stress. *ACS Nano, 5*, 6971–6980.

Shindhal, T., Rakholiya, P., Varjani, S., Pandey, A., Ngo, H. H., Guo, W., Ng, H. Y., & Taherzadeh, M. J. (2021). A critical review on advances in the practices and perspectives for the treatment of dye industry wastewater. *Bioengineered, 12*(1), 70–87.

Surya, K., & Michael, M. S. (2021). Hierarchical porous activated carbon prepared from biowaste of lemon peel for electrochemical double layer capacitors. *Biomass and Bioenergy, 152*, 106175.

Tahir, M. B., Ashraf, M., Rafique, M., Ijaz, M., Firman, S., & Iqra, M. (2020). Activated carbon doped WO_3 for photocatalytic degradation of rhodamine-B. *Applied Nanoscience, 10*, 869–877.

Vesna, V. M., Radojka, R. N., UroŠ, D. M., & Vladimir, S. P. (2014). Removal of cationic and anionic azo dyes from aqueous solutions by adsorption on maize stem tissue. *Journal of the Taiwan Institute of Chemical Engineers*. https://doi.org/10.1016/j.jtice.2013.12.020

Xiaoming, P., Xijun, H., Dafang, F., & Frank, L. Y. L. (2014). Adsorption removal of acid black 1 from aqueous solution using ordered mesoporous carbon. *Applied Surface Science, 294*, 71–80.

Zehra, O., Memduha, E., Deniz, U., & Ayla, Ö. (2019). Green synthesis of biomass-derived activated carbon/Fe-Zn bimetallic nanoparticles from lemon (Citrus limon (L.) Burm. f.) wastes for heterogeneous Fenton-like decolorization of reactive red 2. *Journal of Environmental Chemical Engineering, 7*(4), 103231.

Zhang, W., Xu, M., Zeng, J., Li, J., Li, J., & Xub, X. W. (2013). Superior adsorption capacity of hierarchical iron oxide@magnesium silicate magnetic nanorods for fast removal of organic pollutants from aqueous solution. *Journal Materials Chemistry A, 1*, 11691–11697.